Supporting Information

# Bread-inspired foaming strategy to fabricate wine lees-based porous carbon framework for high specific energy supercapacitor

Hui Peng[‡]*, Yipu Xu[‡], Yaping Jiang, Xin Wang, Rui Zhao, Faqiang Wang, Lu Li, and Guofu Ma*

Key Laboratory of Eco-Functional Polymer Materials of the Ministry of Education, Key Laboratory of Polymer Materials of Gansu Province, College of Chemistry and Chemical Engineering, Northwest Normal University, Lanzhou 730070, China.

‡These authors contributed equally to this work. They should thus be considered co-first authors.

*Corresponding authors. E-mail addresses: penghui@nwnu.edu.cn (H. Peng), magf@nwnu.edu.cn (G. Ma)

**S1. Material Characterization**

The morphologies and structures of the as-prepared samples were characterized by field-emission scanning electron microscopy (FESEM, Carl Zeiss, Ultra Plus, Germany), transmission electron microscopy (TEM, JEM-2010 Japan). The chemical compositions were confirmed on a K-Alpha system (American) using a monochromatic Al Kα radiation source. The crystal structures and defects of samples were examined via X-ray diffraction (XRD, D/Max-2400, Rigaku, k=1.5418 Å, 40 kV, 100 mA) and Raman spectroscopy (Rainie Salt Public Co. Ltd., Britain, 514 nm excitation laser). The Brunauer-Emmett-Teller (BET) surface area of the samples was analyzed by nitrogen adsorption-desorption in a surface area and porosimetry analyzer (ASAP 2020, Micromeritics, U.S.A.). Thermogravimetric analysis was performed on a thermogravimetric analyzer (NETZSCH STA 449 F3) in $N_2$ with a heating rate of 10 $^{o}$C min$^{-1}$.

**S2. Electrochemical measurement**

**Three-electrode system**

Preparation of electrode: The active materials (80 wt %), acetylene black (10 wt %), and binder (poly(tetrafluoroethylene), 10 wt %) were homogeneously mixed in 1-methyl-2-pyrrolidone (NMP) to form a slurry. Then the solution was dropped onto square Ni foam film (1.0×1.0 cm) and dried at 80 $^{o}$C in vacuum overnight. The electrode areal loading is 4-5 mg cm$^{-2}$ and the active material/substrate weight ratio is 0.07-0.09.

Electrochemical test: cyclic voltammetry (CV), galvanostatic charge-discharge (GCD) tests and electrochemical impedance spectroscopy (EIS) tests were performed on the CHI 660D electrochemical workstation within a voltage window of -1-0 V for 2 M KOH electrolytes, respectively. The used counter and reference electrodes are carbon rod electrode and Hg/HgO electrode, and the as-prepared electrode as the working electrode. The specific capacitance charge-discharge measurement was calculated based on the following formula: $C=(I\Delta t)/(m\Delta V)$, where C (F $g^{-1}$) is the specific capacitance, I (A $g^{-1}$) is current density, $\Delta t$ (s) is discharge time, m (g) is the mass of a single electrode, and $\Delta V$ (V) is the potential window during the discharge process.

**Two-electrode system**

In the two-electrode symmetric systems (CR2032), symmetric supercapacitor was assembled by two electrodes with the same size and mass of the active material served as positive and negative electrodes, and a glassy fibrous separator. 0.5 M $Na_2SO_4$, 2.0 M KOH aqueous solutions and [Emim]$BF_4$ ionic liquid were employed as electrolyte respectively. The corresponding electrochemical performance test is the same as the three-electrode system. The electrode areal loading is 4-5 mg $cm^{-2}$ and the active material/substrate weight ratio is 0.07-0.09.

The specific capacitance is counted as $C = (4I\ \Delta t) / (m\ \Delta V)$, where C (F $g^{-1}$) is specific capacitance, I (A $g^{-1}$) is the discharge current density, $\Delta t$ (s) is the discharge time, m (g) is the total mass of positive and negative electrodes for two-electrode cells, and $\Delta V$ (V) is the potential window. The specific energy density (E, Wh $kg^{-1}$) and power density (P, W $kg^{-1}$) for a symmetric supercapacitor were calculated using equation: $E = 1/2CV^2$ and $P = E/t$, where C (F $g^{-1}$) is the specific capacitance of symmetric supercapacitor, V (V) is voltage change during the discharge process and t (s) is the corresponding discharge time.

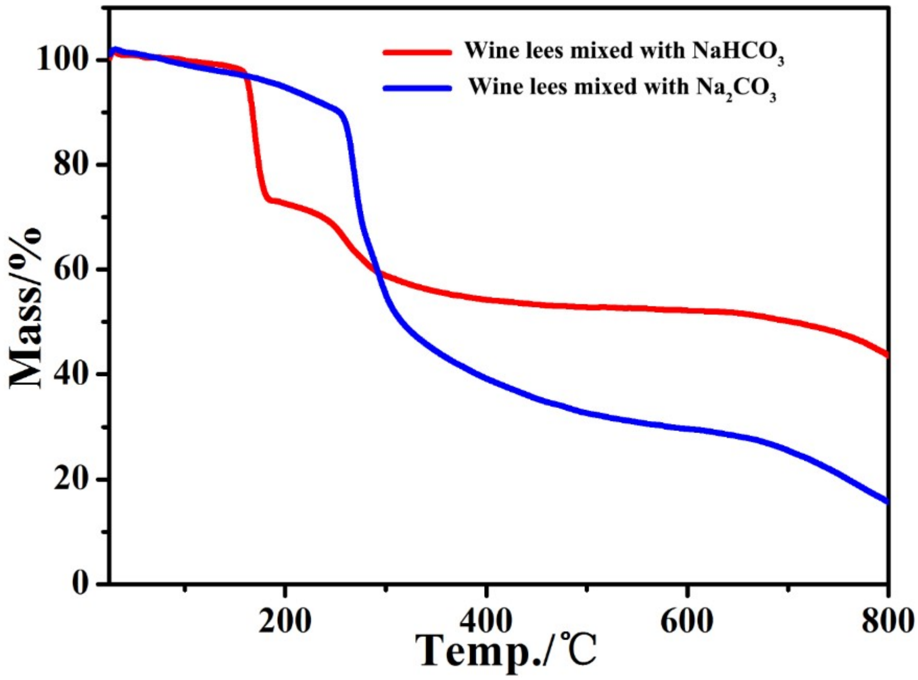


**Figure S1** TGA curves of the precursors heated under $N_2$ atmosphere.

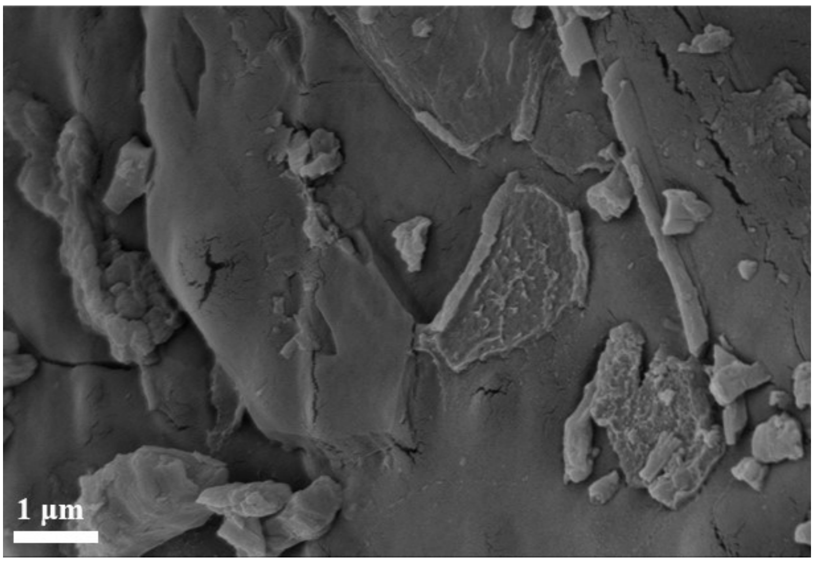


**Figure S2** SEM images of the wine lees.

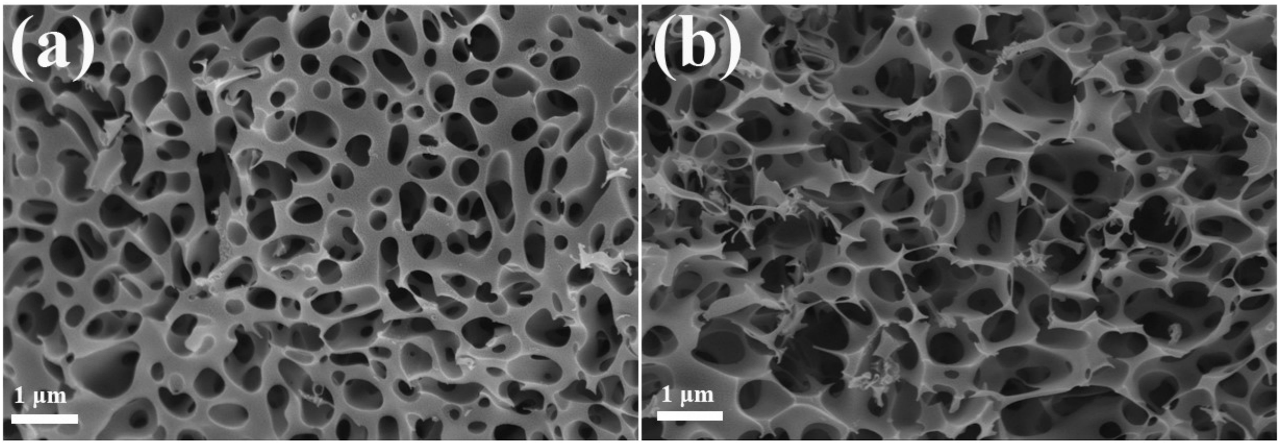


**Figure S3** SEM images of the (a) WLCF-1 and (b) WLCF-3.

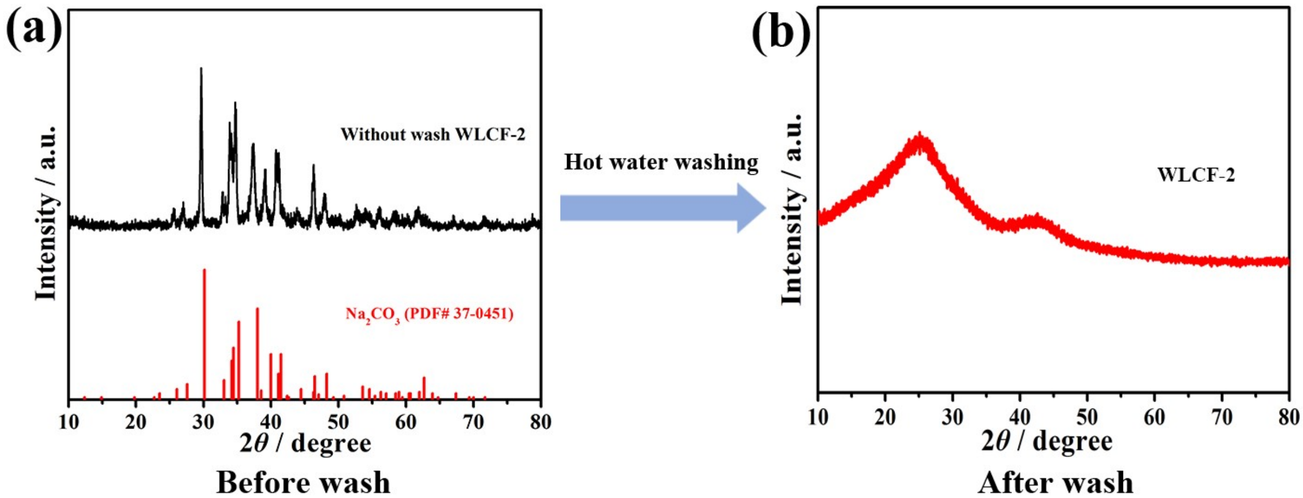


**Figure S4** The XRD pattern comparisons of the WLCF-2 of (a) before and (b) after washing.

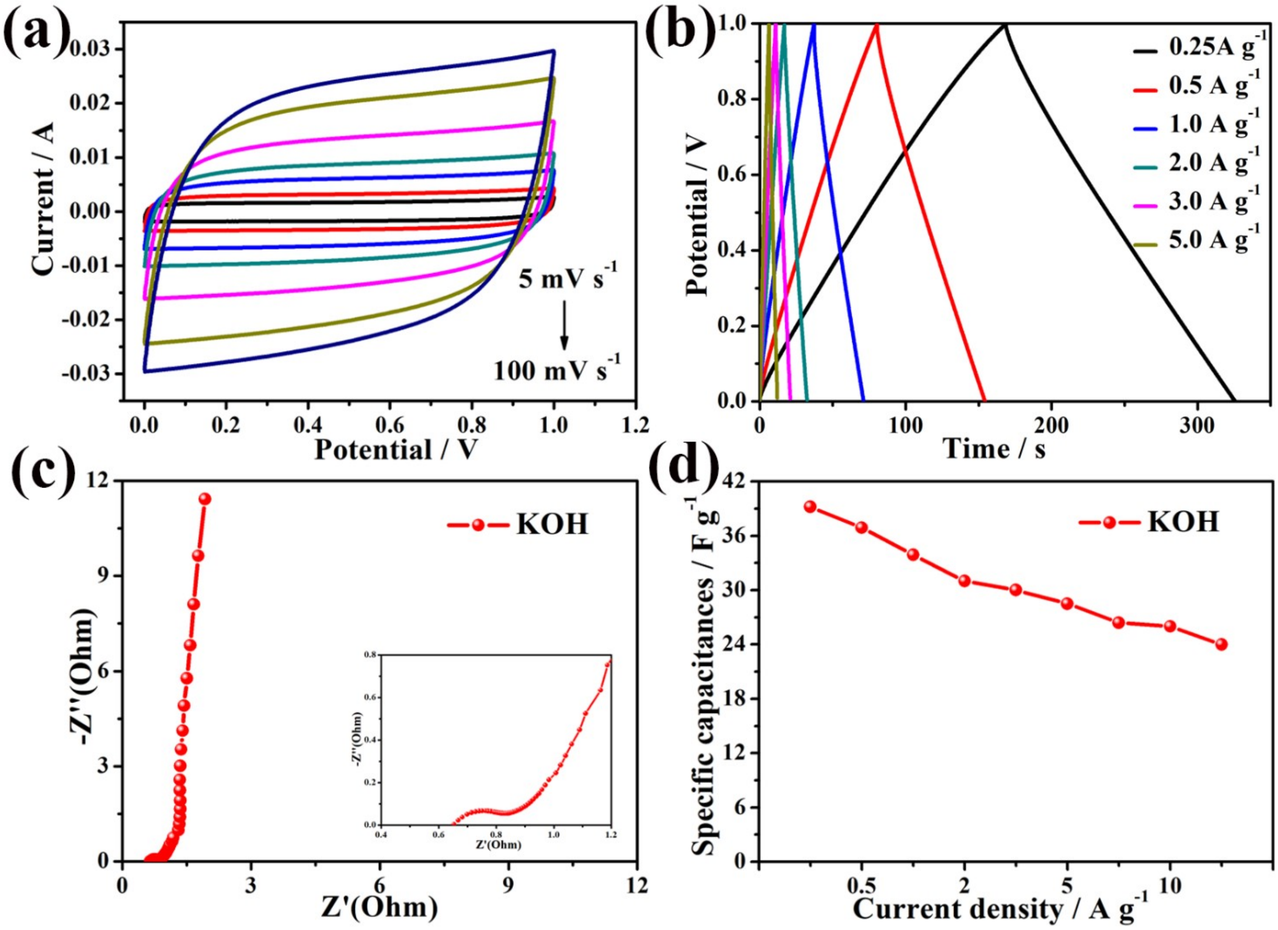


**Figure S5** (a) CV curves of the supercapacitor in KOH electrolyte at different scan rates; (b) GCD curves of the supercapacitor in KOH electrolyte at various current densities; (c) Nyquist plots and (d) the corresponding discharge capacitances of the supercapacitor in KOH electrolyte.

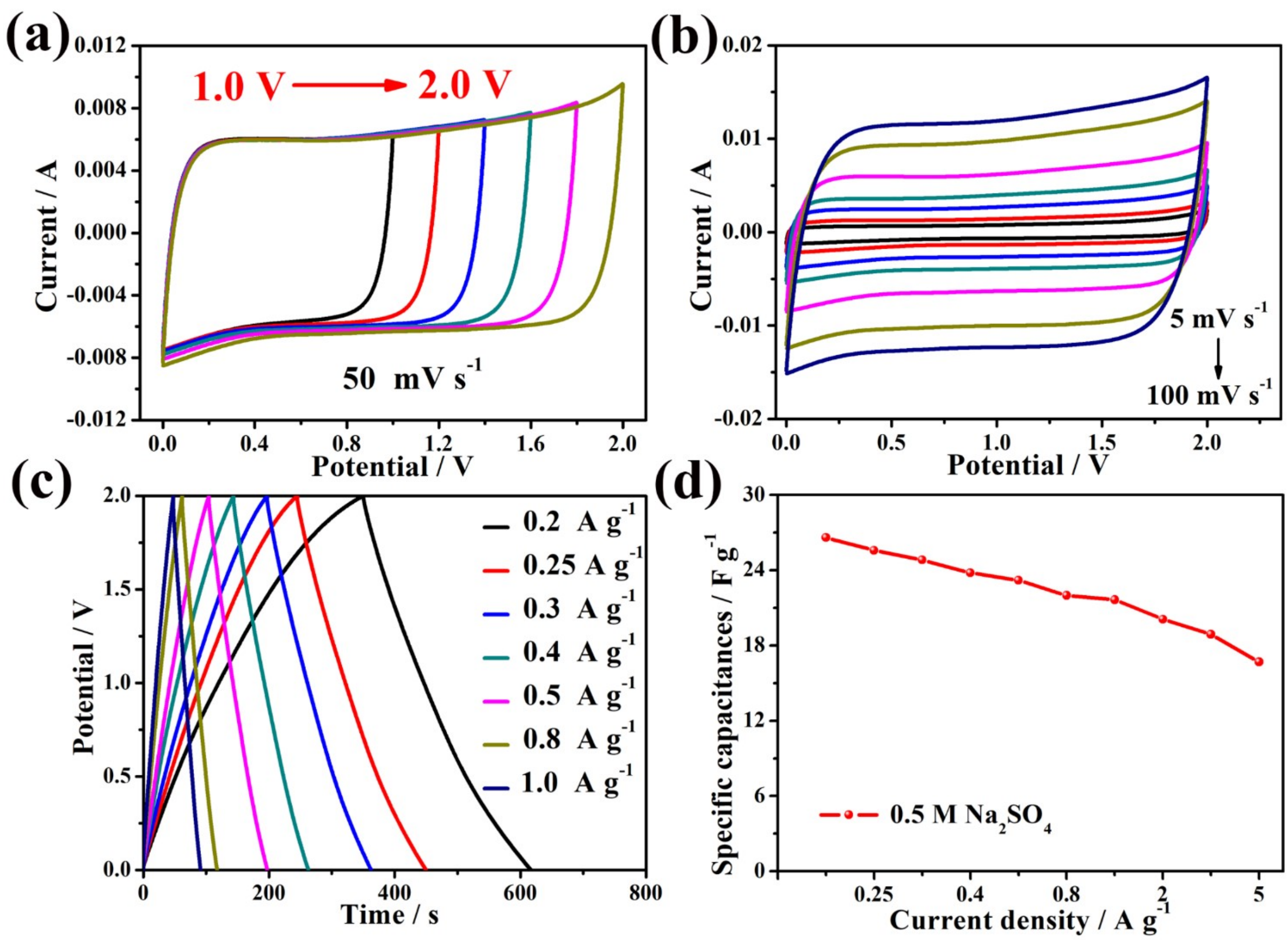


**Figure S6** (a) CV curves of o supercapacitor at different voltage in 0.5 M $Na_2SO_4$ electrolyte; (b) CV curves of the supercapacitor in $Na_2SO_4$ electrolyte at various scan rates; (c) GCD curves of the supercapacitor in $Na_2SO_4$ electrolyte at various current densities and (d) the corresponding discharge capacitances of the supercapacitor in $Na_2SO_4$ electrolyte.

**Table S1.** BET surface area, pore structure parameters, element contents and the XRD data of carbon materials.

| Samples | $S_{BET}$ ($m^2$ $g^{-1}$) | Pore volume ($cm^3$ $g^{-1}$) | Average pore size (nm) | C (wt %) | N (wt %) | O (wt %) | $d_{002}$ (nm) |
|---|---|---|---|---|---|---|---|
| WLCF-0 | 473.5 | 0.54 | 4.58 | 80.17 | 9.27 | 10.56 | 0.347 |
| WLCF-1 | 840.6 | 0.55 | 3.39 | 80.09 | 8.72 | 11.19 | 0.350 |
| WLCF-2 | 1494.6 | 0.76 | 2.05 | 80.76 | 8.21 | 11.03 | 0.353 |
| WLCF-3 | 954.7 | 0.59 | 2.46 | 84.85 | 5.02 | 10.13 | 0.359 |
| WLC | 1106.1 | 0.56 | 2.01 | 80.10 | 8.18 | 11.72 | 0.341 |

**Table S2**. Performances comparison of symmetric cells used various carbon materials in the references.

| Carbon-based materials | Working voltage | Electrolyte | E (Wh kg$^{-1}$) | P (W kg$^{-1}$) | Refs. |
|---|---|---|---|---|---|
| Wine lees-derived carbon framework (WLCF) | 2.0 V | 0.5 M $Na_2SO_4$ | 18.0 | 225 | This work |
| | 4.0 V | $EMIMBF_4$ | 54.0 | 401 | |
| pomelo peels-derived carbon microsheets (PPCs) | 1.6 V | 1 M $Na_2SO_4$ | 11.7 | 160 | [S1] |
| N/P codoped hierarchical porous carbons (NPHCs) | 1.6 V | 1 M $Na_2SO_4$ | 10.61 | 400 | [S2] |
| N-doped carbon (NC) | 1.0 V | 6 M KOH | 7.3 | 125.1 | [S3] |
| hemicellulose-derived porous activated carbon (HPAC) | 1.0 V | $H_2SO_4$/PVA | 11.7 | 349.9 | [S4] |
| N-doped black liquor-derived porous carbons (N-BLPC) | 1.0 V | 6 M KOH | 9.34 | 250 | [S5] |
| Nitrogen-doped hierarchical porous carbon (NHPC) | 0.7 V | 6 M KOH | 9.43 | 630 | [S6] |
| activated nitrogen-doped porous carbons (ANPCs) | 1.8 V | 0.5 M $Na_2SO_4$ | 12.5 | 450 | [S7] |
| Medulla tetrapanacis-derived O/N co-doped porous carbon (MT-900) | 1.8 V | 1.0 M $Na_2SO_4$ | 14.3 | 465.9 | [S8] |
| Nitrogen-doped nanostructure carbon (N-HNC) | 1.0 V | 6 M KOH | 15.99 | 500 | [S9] |
| Nitrogen/sulfur co-doped porous carbons (NSPCs) | 3.0 V | 1.0 M $EMTMPF_6$ | 30.6 | 468.8 | [S10] |
| Nitrogen and oxygen enriched hierarchically porous carbon (NOHPCs) | 2.8 V | 1.0 M TEATFB | 31.4 | 350.9 | [S11] |
| Boron doping carbon materials | 3.0 V | $EMIMBF_4$/AN | 42 | 4500 | [S12] |

## References


S1. Wang, Z.; Tan, Y.; Yang, Y.; Zhao, X.; Liu, Y.; Niu, L.; Tichnell, B.; Kong, L.; Kang, L.; Liu, Z.; Ran, F. Pomelo peels-derived porous activated carbon microsheets dual-doped with nitrogen and phosphorus for high performance electrochemical capacitors. *J. Power Sources* **2018,** *378*, 499-510.

S2. Zhang, Y.; Sun, Q.; Xia, K.; Han, B.; Zhou, C.; Gao, Q.; Wang, H.; Pu, S.; Wu, J. Facile synthesis of hierarchically porous N/P codoped carbon with simultaneously high-level heteroatom-doping and moderate porosity for high-performance supercapacitor electrodes. *ACS Sustain. Chem. Eng.* **2019,** *7* (6), 5717-5726.

S3. Guo, D.; Qian, J.; Xin, R.; Zhang, Z.; Jiang, W.; Hu, G.; Fan, M. Facile synthesis of nitrogen-enriched nanoporous carbon materials for high performance supercapacitors. *J. Colloid Interface Sci.* **2019,** *538*, 199-208.

S4. Lin, H.; Liu, Y.; Chang, Z.; Yan, S.; Liu, S.; Han, S. A new method of synthesizing hemicellulose-derived porous activated carbon for high-performance supercapacitors. *Microporous Mesoporous Mater.* **2020,** *292*, 109707.

S5. Zhu, L.; Shen, F.; Smith, R. L.; Yan, L.; Li, L.; Qi, X. Black liquor-derived porous carbons from rice straw for high-performance supercapacitors. *Chem. Eng. J.* **2017,** *316*, 770-777.

S6. Zeng, R.; Tang, X.; Huang, B.; Yuan, K.; Chen, Y. Nitrogen-doped hierarchically porous carbon materials with enhanced performance for supercapacitor. *ChemElectroChem* **2018,** *5* (3), 515-522.

S7. Lin, G.; Ma, R.; Zhou, Y.; Liu, Q.; Dong, X.; Wang, J. KOH activation of biomass-derived nitrogen-doped carbons for supercapacitor and electrocatalytic oxygen reduction. *Electrochim. Acta* **2018,** *261*, 49-57.

S8. Liu, B.; Yang, M.; Yang, D.; Chen, H.; Li, H. Medulla tetrapanacis-derived O/N co-doped porous carbon materials for efficient oxygen reduction electrocatalysts and high-rate supercapacitors. *Electrochim. Acta* **2018,** *272*, 88-96.

S9. Shang, Z.; An, X.; Zhang, H.; Shen, M.; Baker, F.; Liu, Y.; Liu, L.; Yang, J.; Cao, H.; Xu, Q.; Liu, H.; Ni, Y. Houttuynia-derived nitrogen-doped hierarchically porous carbon for high-performance supercapacitor. *Carbon* **2020,** *161*, 62-70.

S10. Han, J.; Li, Q.; Peng, C.; Shu, N.; Pan, F.; Wang, J.; Zhu, Y. Increasing S dopant and specific surface area of N/S-codoped porous carbon by in-situ polymerization of PEDOT into biomass precursor for high performance supercapacitor. *Appl. Surf. Sci.* **2020,** *502*, 144191.

S11. Yan, W.; Meng, Z.; Zou, M.; Miao, H.; Ma, F.; Yu, R.; Qiu, W.; Liu, X. Y.; Lin, N. Neutralization reaction in synthesis of carbon materials for supercapacitors. *Chem. Eng. J.* **2020,** *381*, 122547.

S12. Chen, D. D.; He, Z. Q.; Wang, M.; Wu, D.; Chen, X. Y.; Zhang, Z. J. Boron doping and structure control of carbon materials for supercapacitor application: the effect of freeze-drying and air-drying for porosity engineering. *J. Solid State Electr.* **2020,** *24* (3), 641-654.